Influence of annealing on the electrical characteristic of GaSbBi Schottky diodes

Zhongming Cao[1], Tim D. Veal[2], Mark J. Ashwin[3], Karl Dawson[4] and Ian Sandall[1*]

1. Department of Electrical Engineering and Electronics, University of Liverpool, Brownlow Hill, Liverpool, L69 3GJ, UK.
2. Department of Physics and Stephenson Institute for Renewable Energy, University of Liverpool, Liverpool, L69 7ZF, UK
3. Department of Physics, University of Warwick, Gibbet Hill, Coventry, CV4 7AL, UK
4. Imaging Centre at Liverpool, University of Liverpool, Brownlow Street, L69 3GL, UK

*Corresponding Author Email: Ian.Sandall@Liverpool.ac.uk

Abstract: The influence of post-growth thermal annealing on GaSbBi Schottky barrier diodes has been investigated. The effects of the annealing temperature and time on the material quality and electrical characteristics of the diodes have been studied. The I-V characteristics indicated a better ideality factor and less leakage current at the reverse bias, as the annealing temperature increased up to 500 °C for a duration of 30 minutes. X-ray diffraction (XRD) and scanning transmission electron microscope (STEM) measurements were performed to verify that the bismuth composition was unaffected during the annealing process. Energy dispersive x-ray (EDX) analysis indicated Sb clustering occurs at high annealing temperatures, resulting in a concomitant degradation in the electrical performance. The optimum electrical characteristics of the diode were obtained with an annealing temperature of 500 °C for 30 minutes, resulting in an ideality factor of 1.3 being achieved.

Keywords: GaSbBi; Schottky diode; electrical characteristics; annealing

1. Introduction

Group III-V bismuth alloys have shown great promise in the past decade as being able to extend the operational wavelength of optoelectronic devices [1-4] due to a large bandgap reduction with only small concentrations of bismuth. This makes dilute bismuth Sb-based semiconductor materials attractive for optoelectronic device applications operating across the near- and mid-infrared spectral ranges[5]. GaSb is typically used in optoelectronic devices working in the near-infrared, such as gas and chemical sensing [6-8]. However, standard type-1 GaSb based laser diodes, comprising of GaInAsSb Quantum Wells with AlGaAsSb barriers suffer from a low valence band offset at the interface, resulting in high hole leakage, this problem becomes more significant as the composition of the alloys are adjusted for longer wavelength emission, due to the quantum well valance level reducing as the As fraction is increased [9,10].

Introducing small amounts of Bi into GaSb can significantly reduce the band gap and thus potentially extend the emission wavelength to beyond 3 μm, opening up new applications in biological and chemical sensing. While the reduction in the bandgap is primarily due to a downward shift in the conduction band there is also a concomitant raising of the valence band [11-15], which may help to supress hole leakage in GaSb-based laser devices[16].

However, successful incorporation of Bi into the GaSb matrix requires non-standard growth parameters such as very low growth temperatures, potentially reducing the quality of the material. As such, obtaining high Bi incorporation while still retaining a high crystal quality remains a challenge that has not been fully addressed and optimised.

Despite significant research over recent years focused on introducing Bi into GaAs [17-19], primarily driven to achieve more efficient laser diodes for telecommunications operation, there has been little attention paid to GaSb based alloys. GaAsBi alloys also require a non-standard growth parameter space and as such a number of refinements and advances to the

growth and subsequent fabrication have had to be realized to enable functioning laser diodes to be obtained. For example, Marko et al.[18] studied the optical gain spectra of GaAsBi/(Al)GaAs quantum wells to obtain optimal internal optical losses of 10-15 cm^{-1} and modal gain of 24 cm^{-1} . While Feng et al.[20] have investigated the influence of annealing on the optical properties of $GaAs_{0.968}Bi_{0.032}$ by photoluminescence intensity and HR-XRD measurements which were performed to characterize the structural changes during annealing, this showed the PL peak intensities remain stable for annealing temperatures of up to 700 °C, and then severely deteriorate at 800 °C.

Comparatively, there are only a few articles reported on Bi incorporation in GaSb [5,15,21-24], especially the electrical properties of GaSbBi. Rajpalke et al. [25] have realized $GaSb_{1-x}Bi_x$ material by molecular beam epitaxy with 9.6% Bi incorporation, with droplet-free smooth surfaces and high crystalline quality, resulting in a band gap of 410 meV. More recently, even higher Bi contents in the range 11-14.5% have been demonstrated by Delorme et al. [5], Yue et al. [26] and Hilska et al. [27]. To try and achieve better electrical performance Dier et al. [28] and Rotelli at al. [29] have investigated various passivation processes to reduce oxide layers on the surface of GaSb. Recently a GaSbBi-based laser diode has been demonstrated [30]; this had an extended emission wavelength of 2.5 μm at 80 K and 2.7 μm at room-temperature but at a high threshold current density of 431 A/cm^2 and 4.22 kA/cm^2, respectively, indicating a high level of defects and leakage mechanisms originating from the introduction of Bi to the GaSb matrix. As such, while lasing devices have been demonstrated, there is still significant work needed to optimize and improve the material quality to realize efficient laser sources for device applications.

In this work, thin films of GaSbBi films were grown by molecular beam epitaxy and subsequently fabricated into Schottky diodes. The effect of post-growth annealing on the physical properties of the material and subsequent electrical properties of the devices was

investigated as a potential method to improve the material quality and hence its electrical performance.

2. **Experimental**

A series of thin GaSbBi films were grown using molecular beam epitaxy (MBE) on GaSb substrates. The samples were grown using a Mod Gen II using a cracker cell to provide the Sb flux and Vecco Sumo cells to provide the Bi and Ga fluxes, It is assumed that the Sb fluxes comprises Sb_2 for the valve temperature of 800°C. The samples consisted of 400 nm thick nominally undoped GaSbBi layers grown on 100 nm-thick GaSb buffer layers grown directly onto the substrate. Samples with Bi concentrations of 3.5% and 4% were grown at a temperature of 325 and 250 °C, respectively, with growth rates of 0.75 μm/h and 0.5 μm/h. The Bi content of the GaSbBi films was determined using x-ray diffraction (XRD) using the fact that we have previously quantified the dependence of lattice parameter on Bi content by combining XRD and Rutherford backscattering.[25] The XRD measurements in this work used a Rigaku Smartlab x-ray diffractometer, with a rotating copper anode and Ge (220) four bounce monochromator, under ambient conditions. The Cu $K\alpha_1$ line was used with a wavelength of 1.5406 Å. The 004 Bragg reflections were measured. A series of reference GaSb samples was grown where a nominally undoped 400nm layer of GaSb was grown at temperatures of 250, 300, 325 and 400 °C.

Epitaxial wafers were initially cleaved and then cleaned with acetone and isopropyl alcohol for 10 mins each. The samples were annealed with different temperatures and time, under a nitrogen rich background in an annealing furnace. The samples were sandwiched between two dummy GaSb wafers and placed in a sealed ampoule during the annealing process to prevent out-diffusion of Sb. The Ohmic contact of the backside was made by evaporating Au-Zn-Au, before patterning of the top contact via photolithography. The top Schottky contact

consisted of Ti-Au and was deposited via thermal evaporation. Electrical, current-voltage (I-V) measurements were performed with an Agilent Technology B1500A Semiconductor Device Analyser.

To investigate this more closely, we have performed transmission electron microscopy (TEM) on the samples to look for changes in the material as the anneal temperature is increased.

For Transmission Electron Microscopy (TEM) measurements, electron transparent thin lamella specimens were prepared from wafer sections, using the focussed ion beam (FIB) lift-out method[31], using a dual beam FEI Helios 600i FIB instrument. Trenching and thinning were performed using a 30kV Ga ion beam before damaged surface layers were removed with a 5kV beam.

Bright field (BF) and high angle annular dark field (HAADF) images were recorded using a probe side aberration corrected JEOL 2100FCs scanning transmission electron microscope (STEM) operating at 200keV. HAADF z-contrast images were formed using electrons collected over a semi-angle range from 70 to 190 mrad. Energy dispersive x-ray spectroscopy was performed, in the TEM, using an EDAX windowless x-ray detector.

3. Results and discussion

As GaSbBi films have to be grown at low temperatures in order to incorporate Bi, we initially measured a series of Schottky diodes fabricated from GaSb thin films grown at different temperatures. This series of samples was grown on p-type GaSb substrates and consisted of 400 nm thick nominally undoped GaSb layers. The I-V characteristics of the resultant diodes are shown in Fig. 1. As the growth temperature decreases there is a significant decrease in the diode rectification, with non-diode like I-Vs being observed at growth temperatures below 400 $^{\circ}$C. Similar results have been obtained previously [32] and were attributed to the low surface

mobility of elemental antimony at these growth temperatures, resulting in Sb having an increased probability of being incorporated at antisites.

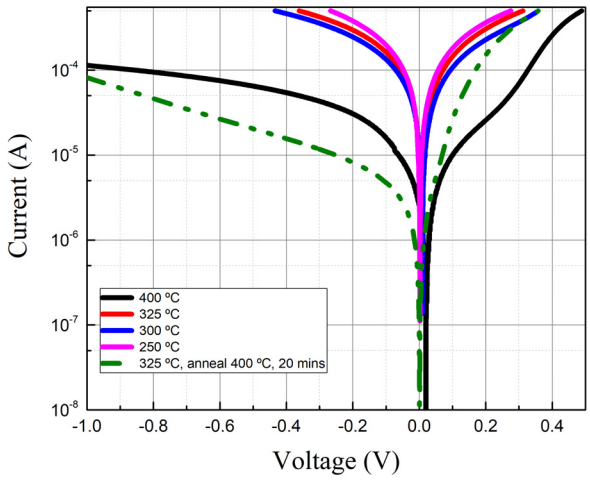

Fig. 1 I-V characteristic of Au/GaSb Schottky diodes for different GaSb growth temperatures and also after post-growth annealing.

We then performed post-growth annealing on samples grown at low temperatures to see if improved electrical performance could be obtained. The I-V characteristic for the diode grown at 325 °C and then subsequently annealed at 400 °C for 20 mins is also shown in figure 1 (dashed line). This confirms that the electrical properties of low growth temperature GaSb can be dramatically improved by a subsequent annealing process. The results shown in figure 1, indicate that the annealed low growth temperature sample actually has better diode characteristics than the corresponding high growth temperature sample. Similar annealing results have been reported previously on different materials, such as GaN [33] and more recently GaAsBi[20].

The annealing process was then repeated to see if similar annealing could improve the performance of GaSbBi devices grown, for initial measurements the samples with a Bi composition of 3.5% (corresponding to a growth temperature of 325 °C) were utilized.

Samples were annealed at temperatures of between 400 and 500 °C for durations between 5 and 30 minutes. To initially verify that the annealing process has not altered the Bi concentration, x-ray diffraction (XRD) measurements were performed on each of the GaSbBi samples.

The XRD patterns of the GaSbBi for the as-grown reference layer and layers annealed at 400 and 500 °C for 30 mins are shown in Fig. 2 (symbols), along with corresponding simulations (lines). It can be seen that the peak corresponding to the GaSbBi film is at a lower angle than the substrate GaSb. This corresponds to the expansion of the lattice of the GaSbBi epilayers with respect to the substrate [14]. Good simulation were obtained for each of the samples using the film thickness and Bi content parameters given in Table I. It is clear from the XRD that the main epilayer peak does not shift significantly during the annealing process, the simulation result indicates the bismuth incorporation is unaffected by the annealing procedures. To within the accuracy of the modelling of the XRD data, the film thickness is constant for all annealing treatments apart from 500°C for 30 minutes. For that one annealing treatment, the deduced change may be a real change of GaSbBi layer thickness due to out diffusion of Bi, but the apparent change in film thickness may instead be a manifestation in the XRD modelling, we will revisit this result at the end of the paper to discuss it further.

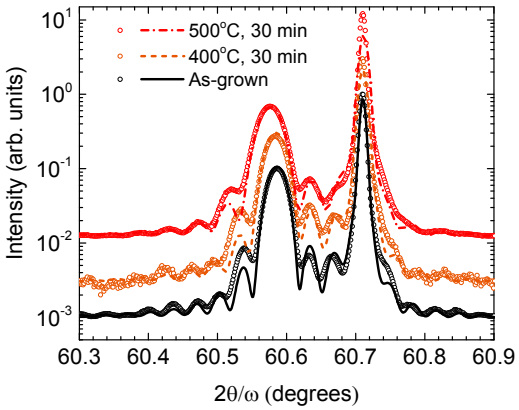

Fig. 2 XRD patterns of the 004 reflections of GaSbBi films containing 3.5% Bi with different annealing temperatures. The experimental data are shown as open circles and the simulations are shown as lines.

Table I. The parameters used to model the XRD patterns after different annealing treatments.

Annealing temperature (°C)	Annealing time (minutes)	Film thickness (nm) ± 10 nm	Bi content (% of anion sublattice) ± 0.10
As - grown	As - grown	308	3.45
400	30	290	3.45
500	5	290	3.15
500	15	290	3.70
500	30	245	3.70

To investigate potential improvements in the electrical performance, the same samples were fabricated into Schottky diodes and room temperature I-V measurements were performed, with the results shown in figure 3. It can be seen that the diode characteristics are improved upon annealing, with lower dark currents being observed as a function of both increasing annealing temperature and time, resulting in the device annealed at 500 °C for 30 mins showing good diode-like behaviour. We have fitted the experimental data with the diode equation to enable us to extract the ideality factor and saturation current for the diodes as a function of annealing the condition. Figure 4a gives the values obtained for devices annealed for 15 mins while figure 4b, gives the values for those annealed for 30 mins. For the samples annealed for 15 minutes, the values of saturation current decreased from 2.64×10^{-4} A (as-

grown) to 1.68×10^{-5} A (at 500 °C), and the ideality factor decreased from 2.57 (as-grown) to 1.62 (at 500 °C). A similar trend can be observed (fig. 4b) for devices annealed for 30 minutes with the saturation current and the ideality factor decreased to 3.72×10^{-5} A and 1.3, respectively, after annealing at a temperature of 500 °C. The extracted values of the ideality factor are relatively high, particularly for the as-grown sample. This suggests that the dominant recombination process in these diodes is not thermionic emission [34,35], but rather other current processes are actively contributing to the diode performance. These additional current paths could come from a range of potential sources including, but not limited to, surface roughness, tunnelling due to high background doping, impurities or the presence of native oxide layers. The improvement in the I-V curves observed in figure 3, suggest that dislocations or point defects which are subsequently repaired upon annealing [36,37] may well be contributing to these additional current paths. The full analysis of these possible current mechanisms is beyond the scope of this current paper, however, this does not take away from the key result obtained here that post-growth annealing can significantly improve the diode performance and its extracted ideality factor. These results also indicate longer annealing times, at least up to 30 minutes results in an improved electrical performance compared to shorter times. Of course the optimum annealing conditions will be determined by the thermal dose induced in the sample, which will be a function of temperature and time. These results show that post-growth annealing can result in dramatically improved electrical performance of GaSbBi alloys.

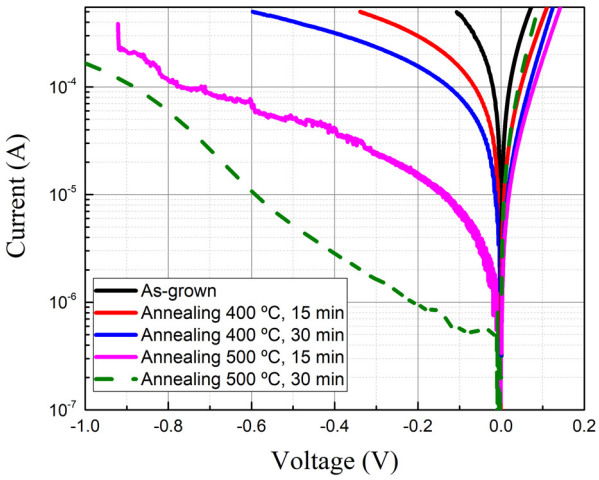

Fig. 3 I-V characteristics of Au/GaSbBi containing 3.5% Bi Schottky diode after different annealing condition

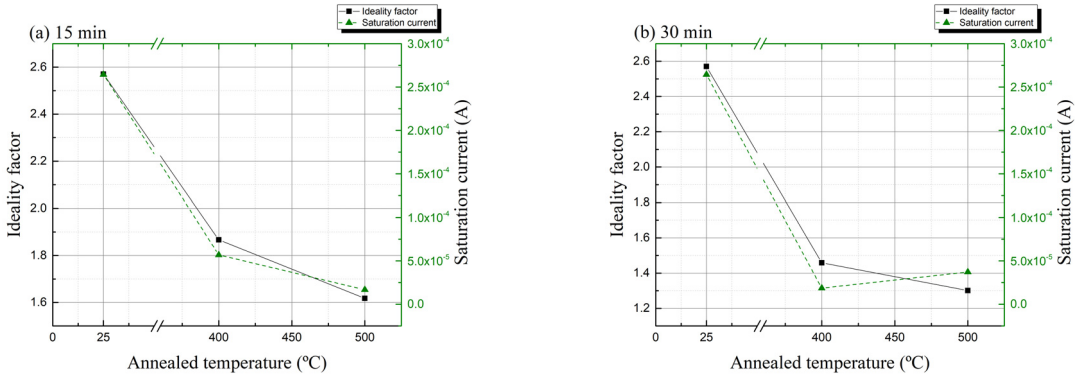

Fig. 4 Temperature dependent ideality factor and saturation current of Au/GaSbBi containing 3.5% Bi Schottky diode under different annealing conditions (a) 15 min and (b) 30 min

To investigate the repeatability of this result as well as the influence of higher annealing temperatures, an additional sample with a Bi composition of 4%, was also annealed and the measurements were repeated. The resultant I-V characteristics of the Schottky diodes are presented in Fig. 5. As before, a clear improvement is observed in the diode characteristics as the annealing temperature increased to 500 ˚C. However, when the annealing temperature increases further to 550 ˚C, a resultant deterioration in the electrical performance is noted. From fitting the experimental data, similar reductions in the ideality factor and saturation current (presented in figure 5b), are interesting to note that electrical properties initially

degrade (higher saturation current and ideality factors) as the sample is annealed up to a temperature of 450 °C, which is in contrast to the results noted on the previous sample. The most likely explanation for this is non-uniformity across the wafer, potentially leading to a higher number of defects in the sample annealed at 450 °C. This seems particularly likely as this piece of the wafer originated much closer to the wafer edge than the other pieces that were annealed.

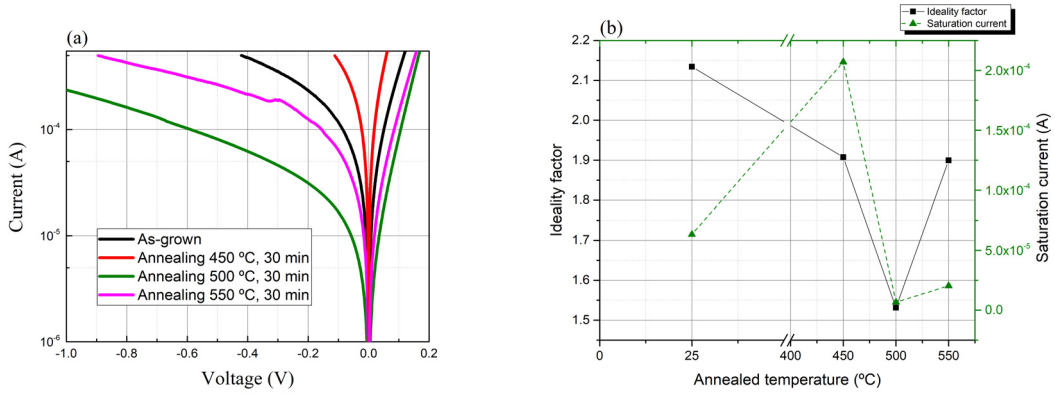

Fig. 5 (a) I-V characteristics of Schottky diode sample with 4% Bi at differing annealing temperatures and (b) extracted ideality factor and saturation currents

While this result confirms the previous result and indicates that annealing can help improve the electrical performance, it also suggests that a secondary process is also occurring during the annealing process. Initially upon annealing the material quality is improved, leading to improved electrical performance. However, as the temperature is increased, a second change in the material occurs which has a detrimental effect on the electrical performance. To investigate this more closely, we have performed transmission electron microscopy (TEM) on the samples with a Bi content of 4% to look for changes in the material as the anneal temperature is increased.

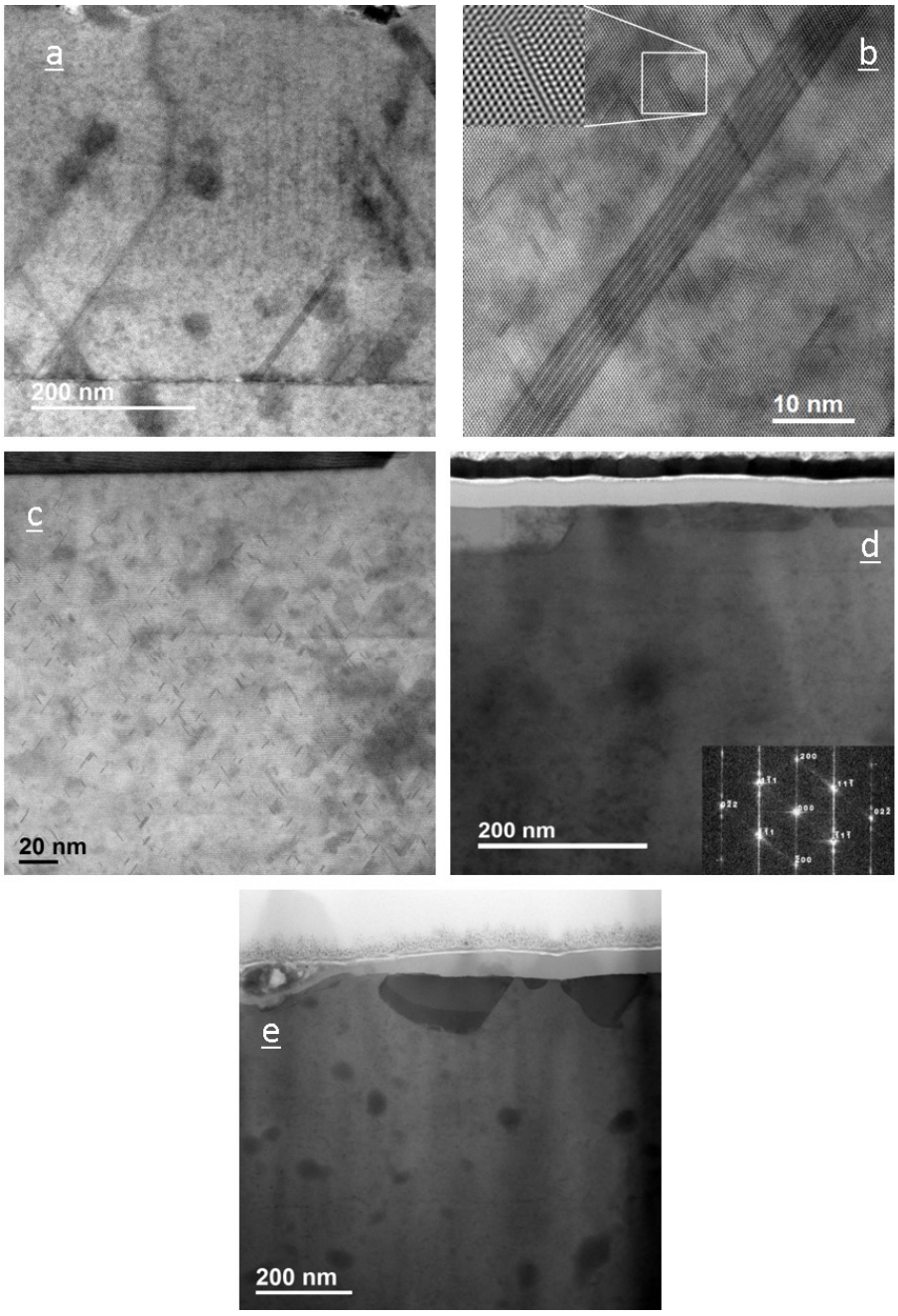

Fig. 6 TEM image of Au/GaSbBi Schottky diode under different annealing conditions (a) as-grown sample, (b) zoomed in image of as-grown sample with atom scale image of crystal matrix in the inset, (c) annealed at 450 ºC, (d) annealed at 500 ºC, with inset showing FFT intensity and (e) sample annealed at 550 ºC.

Figure 6 shows TEM images from the various samples. From the as-grown sample (figure 6a), a large number of diagonal dislocations can be observed at the interface between the substrate and the epitaxial layer. Figure 6b shows an increased magnification image around the defects with an ultrahigh atomic scale resolution image in the inset. Unidentified features, which appear as crystallographic faults lying parallel to the {111}planes can be observed in the Bi alloyed epilayer. These larger stacking faults range in size between 100 and 200 nm.

For the sample annealed at 450 ºC (figure 6c), a dramatic reduction can be seen in the density of these dislocations, with them only being apparent at length scales less than 10nm. The dislocations appear to have been completely removed by an annealing temperature of 500 ºC (figure 6d). FFT intensities (shown in the inset of figure 6d) are consistent with 011 zone axis orientation of the cubic GaSb F-43m structure [38], indicating high quality crystallographic structure has been obtained. It seems likely these dislocations are one of the key sources of high leakage currents in the devices and that annealing has allowed them to be repaired giving rise to an improved electrical performance. For the sample annealed at 550 ºC (figure 6e) while again there is no evidence of dislocations there does appear to be a further change in the material with some material clustering being observed. Indeed, the lattice parameter obtained from the FFT intensity plot of 6.1180 Å corresponds to a local Bi content of 6.6%, once the elastic constants of GaSb are applied to account for the increased lattice expansion in the growth direction due to pseudomorphic growth. While the XRD of the material annealed at 500°C indicates negligible change in the average Bi content upon annealing, the TEM suggests there are regions locally with much higher Bi content of up to 6.6% Bi.

Energy Dispersive X-ray (EDX) analysis of this (figure 7) suggests that the clustering is due to Sb segregation within the epitaxial layer at these higher annealing temperatures. While less apparent at 500 ºC some small areas of Sb segregation are also observed at this temperature. While the mechanism responsible for this apparent movement of Sb within the sample is not

clear, one possible explanation could be the movement of Sb atoms via vacancies, through the lattice. This change in material composition is likely to account for the subsequent degradation in the electrical performance of the diodes observed in figure 5, at the highest annealing temperatures. We have also utilized the EDX data to further investigate the previous anomaly noted in the XRD (figure 2) data which suggested a potential reduction in the Bi layer thickness upon annealing. Within the accuracy of the TEM and EDX measurements the epitaxial layer thickness does not change after annealing, additionally the Bi composition appears to be uniform in each sample, indicating that Bi out diffusion has not occurred. The movement of the Sb atoms observed in figure 7, and the previously discussed Bi clustering noted from the FFT intensity, are likely to be influencing the observed XRD result in figure 2, as after annealing at the highest temperatures compositional non-uniformity has been introduced to the sample which will influence the experimental data and has invalidated some of the assumptions used in the modelling.

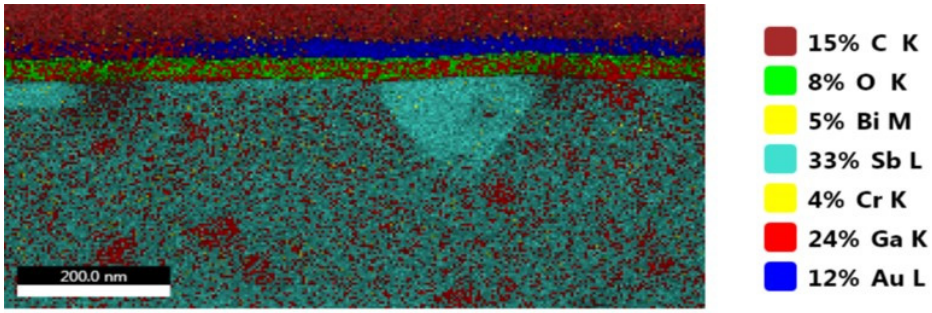

Fig. 7 EDX map of sample annealed at 550 °C

From the TEM and EDX analysis, it appears that upon annealing the stacking faults are repaired within the sample. However, at higher temperatures, subsequent Sb clustering is observed, indicating that the optimum annealing temperature for GaSbBi is between 450 and 500 ºC.

In our previous work[24] we have performed capacitance voltage measurements to extract the doping density in GaSbBi Schottky Diodes, observing a relatively high p-type doping which was in part attributed to acceptor type defects. Utilizing the same approach here we obtain hole densities for the as-grown samples of $3.7 \pm 1.5 \times 10^{18}$ cm^{-2} (for the 3.5% Bi sample) and $7.6 \pm 2.4 \times 10^{18}$ cm^{-2} (for the 4% Bi sample), which are in broad agreement the previous work. After annealing we do not observe any significant change in these values within the uncertainty of the measurement. This appears to suggest that the annealing process has not significantly altered the number of acceptor type defects present, however this result should be treated with some caution for two reasons. Firstly the relatively large uncertainty in the extracted values may be hiding a small change in the doping density, while secondly there may be more than one process taking place during the annealing process with each having a different effect on the overall doping density. For example some of the acceptor based defects may be repaired during the annealing process, leading to a lowering of the doping density, while the annealing temperature may provide sufficient thermal energy to enable other dopants to become active and hence increasing the effective density. A more detailed analysis of the doping density and the influence on annealing is beyond the scope of this current work.

3 Conclusion

In this paper, we presented the electrical performance of Schottky diodes realized from GaSbBi thin films. Improved electrical performance, resulting in an improvement of the ideality factor from 2.6 to 1.3 has been observed after utilizing post-growth annealing at 500 $^{\circ}C$ for 30 min. TEM analysis indicates that this improvement is due to the repair of crystalline dislocations when the sample is annealed. TEM and EDX has also indicated a secondary material change associated with Sb movement/clustering that occurs at higher annealing temperatures, causing a degradation in the electrical performance. This work indicates that

the optimum annealing temperature for GaSbBi alloys is in the range of 450 to 500 °C. These results provide a route for improving the electrical performance of GaSbBi epitaxial layers, which has potential benefits in realizing high performance optoelectronic devices.

References

1 Y. Tominaga, Y. Kinoshita, K. Oe, and M. Yoshimoto, Applied Physics Letters **93,** 131915 (2008).

2 X. Lu, D. Beaton, R. Lewis, T. Tiedje, and Y. Zhang, Applied physics letters **95,** 041903 (2009).

3 M. Ferhat and A. Zaoui, Physical Review B **73,** 115107 (2006).

4 S. Tixier, M. Adamcyk, T. Tiedje, S. Francoeur, A. Mascarenhas, P. Wei, and F. Schiettekatte, Applied physics letters **82,** 2245 (2003).

5 O. Delorme, L. Cerutti, E. Tournie, and J. B. Rodriguez, Journal of Crystal Growth **477,** 144 (2017).

6 F. M. Mohammedy and M. J. Deen, Journal of Materials Science: Materials in Electronics **20,** 1039 (2009).

7 M. Motyka, G. Sęk, K. Ryczko, J. Misiewicz, T. Lehnhardt, S. Höfling, and A. Forchel, Applied Physics Letters **94,** 251901 (2009).

8 L. Ma, W. Hu, Q. Zhang, P. Ren, X. Zhuang, H. Zhou, J. Xu, H. Li, Z. Shan, and X. Wang, Nano letters **14,** 694 (2014).

9 S. D. Sifferman, H. P. Nair, R. Salas, N. T. Sheehan, S. J. Maddox, A. M. Crook, and S. R. Bank, IEEE Journal of Selected Topics in Quantum Electronics **21,** 1 (2015).

10 R. Kudrawiec, J. Kopaczek, O. Delorme, M. Polak, M. Gladysiewicz, E. Luna, L. Cerutti, E. Tournié, and J. Rodriguez, Journal of Applied Physics **125,** 205706 (2019).

11 H. Li and Z. M. Wang, *Bismuth-containing compounds* (Springer, 2016).

12 D. Cooke, F. Hegmann, E. Young, and T. Tiedje, Applied physics letters **89,** 122103 (2006).

13 M. Polak, P. Scharoch, R. Kudrawiec, J. Kopaczek, M. Winiarski, W. Linhart, M. K. Rajpalke, K. Yu, T. Jones, and M. Ashwin, Journal of Physics D: Applied Physics **47,** 355107 (2014).

14 M. K. Rajpalke, W. Linhart, K. Yu, T. S. Jones, M. Ashwin, and T. D. Veal, Journal of Crystal Growth **425,** 241 (2015).

15 M. K. Rajpalke, W. Linhart, M. Birkett, K. Yu, D. O. Scanlon, J. Buckeridge, T. S. Jones, M. Ashwin, and T. D. Veal, Applied Physics Letters **103,** 142106 (2013).

16 L. Shterengas, G. Belenky, J. Kim, and R. Martinelli, Semiconductor science and technology **19,** 655 (2004).

17 H. Kim, Y. Guan, S. E. Babcock, T. F. Kuech, and L. J. Mawst, Journal of Applied Physics **123,** 113102 (2018).

18 I. P. Marko, C. A. Broderick, S. Jin, P. Ludewig, W. Stolz, K. Volz, J. M. Rorison, E. P. O'Reilly, and S. J. Sweeney, Scientific reports **6,** 28863 (2016).

19 R. D. Richards, C. J. Hunter, F. Bastiman, A. R. Mohmad, and J. P. R. David, IET Optoelectronics **10,** 34 (2016).

20 G. Feng, K. Oe, and M. Yoshimoto, Japanese Journal of Applied Physics **46,** L764 (2007).

21 Y. Song, S. Wang, I. Saha Roy, P. Shi, and A. Hallen, Journal of Vacuum Science & Technology B, Nanotechnology and Microelectronics: Materials, Processing, Measurement, and Phenomena **30,** 02B114 (2012).

22 S. Das, T. Das, and S. Dhar, Semiconductor Science and Technology **29,** 015003 (2013).

23 C. R. Tait and J. M. Millunchick, Journal of Applied Physics **119,** 215302 (2016).

[24] N. Segercrantz, J. Slotte, I. Makkonen, F. Tuomisto, I. Sandall, M. Ashwin, and T. Veal, Journal of Physics D: Applied Physics **50,** 295102 (2017).
[25] M. K. Rajpalke, W. Linhart, M. Birkett, K. Yu, J. Alaria, J. Kopaczek, R. Kudrawiec, T. S. Jones, M. Ashwin, and T. D. Veal, Journal of Applied Physics **116,** 043511 (2014).
[26] L. Yue, X. Chen, Y. Zhang, F. Zhang, L. Wang, J. Shao, and S. Wang, Journal of Alloys and Compounds **742,** 780 (2018).
[27] J. Hilska, E. Koivusalo, J. Puustinen, S. Suomalainen, and M. Guina, arXiv preprint arXiv:1901.02687 (2019).
[28] O. Dier, C. Lin, M. Grau, and M.-C. Amann, Semiconductor science and technology **19,** 1250 (2004).
[29] B. Rotelli, L. Tarricone, E. Gombia, R. Mosca, and M. Perotin, Journal of applied physics **81,** 1813 (1997).
[30] O. Delorme, L. Cerutti, E. Luna, G. Narcy, A. Trampert, E. Tournié, and J.-B. Rodriguez, Applied Physics Letters **110,** 222106 (2017).
[31] L. A. Giannuzzi, B. Kempshall, S. Schwarz, J. Lomness, B. Prenitzer, and F. Stevie, in *Introduction to focused ion beams* (Springer, 2005), p. 201.
[32] S. Haywood, N. Mason, and P. Walker, Journal of Crystal Growth **93,** 56 (1988).
[33] P. K. Rao and V. R. Reddy, Materials Chemistry and Physics **114,** 821 (2009).
[34] R. T. Tung, Materials Science and Engineering: R: Reports **35,** 1 (2001).
[35] J. H. Werner and H. H. Güttler, Journal of applied physics **69,** 1522 (1991).
[36] A. Duzik and J. M. Millunchick, Journal of Crystal Growth **390,** 5 (2014).
[37] X. Liu, H. Li, F. Guo, M. Li, and L. Zhao, Physica E: Low-dimensional Systems and Nanostructures **41,** 1635 (2009).
[38] R. Wyckoff, *Crystal Structures* Vol. 1, 2nd ed. (Interscience Publishers, ,New York, 1963).

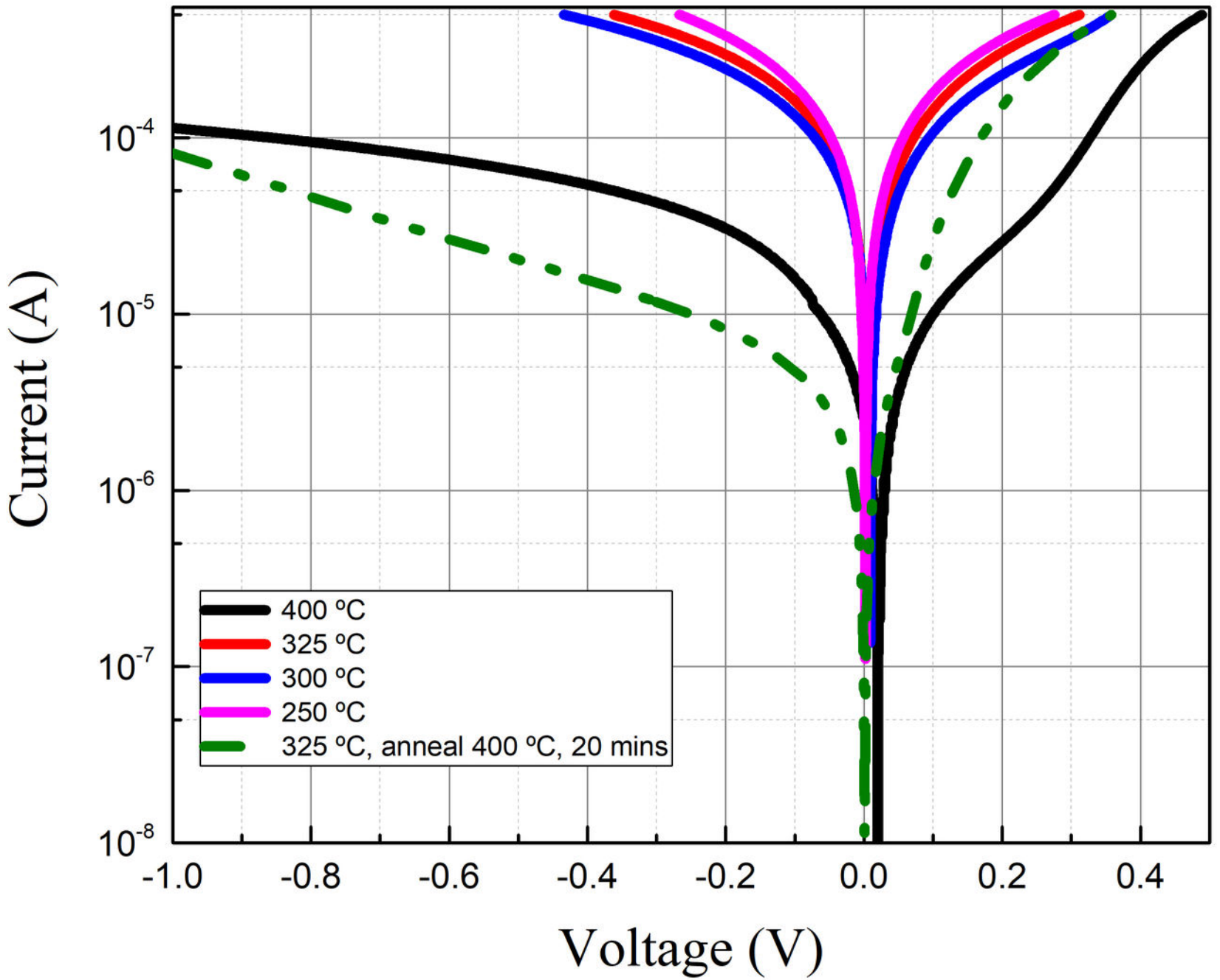
Current (A)
10-4
10-5
10-6
10-7
10-8
-1.0
-0.8
-0.6
-0.4
-0.2
0.0
0.2
0.4
Voltage (V)
400 ºC
325 ºC
300 ºC
250 ºC
325 ºC, anneal 400 ºC, 20 mins

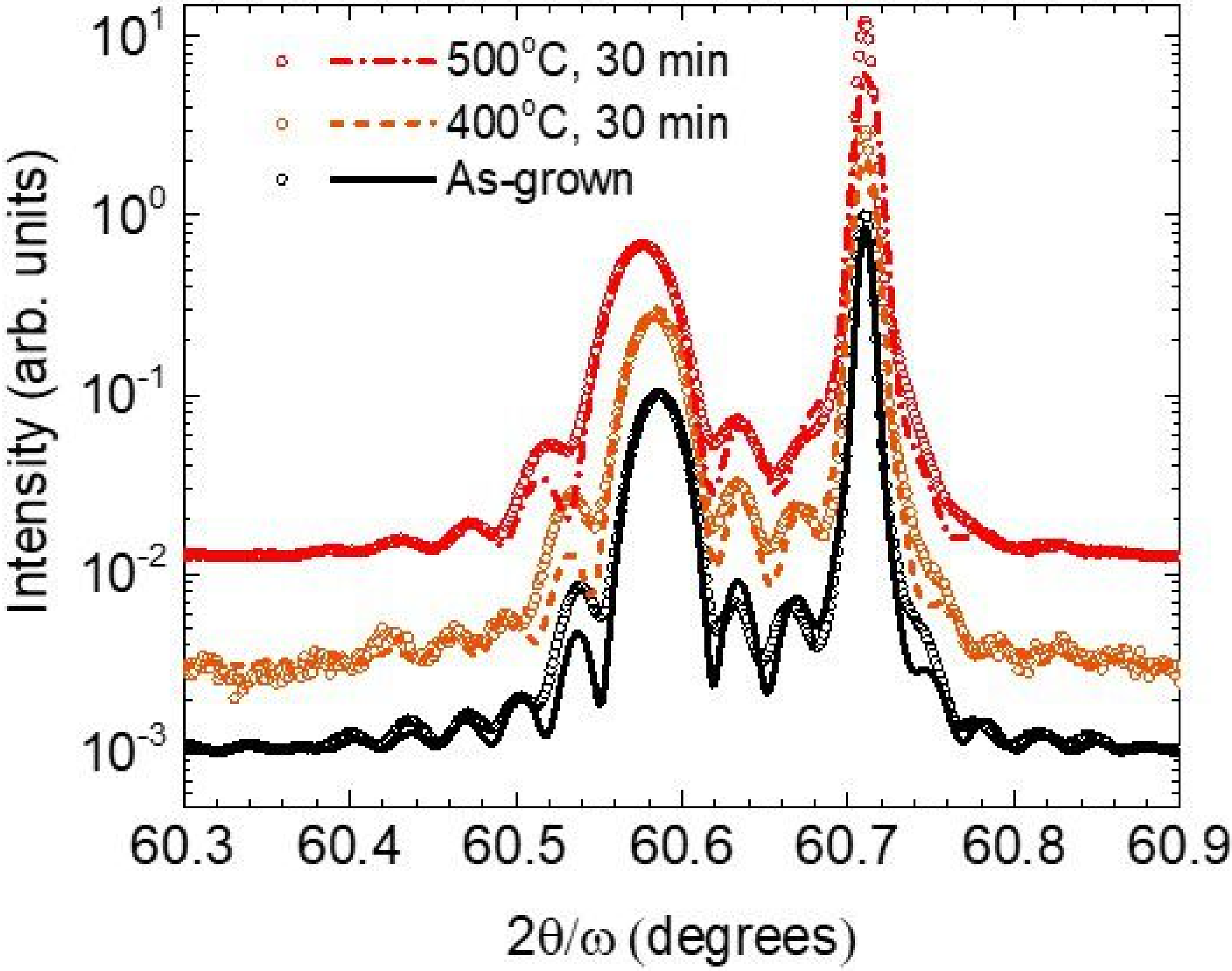
500°C, 30 min
400°C, 30 min
As-grown
Intensity (arb. units)
10^1
10^0
10^-1
10^-2
10^-3
60.3
60.4
60.5
60.6
60.7
60.8
60.9
2θ/ω (degrees)

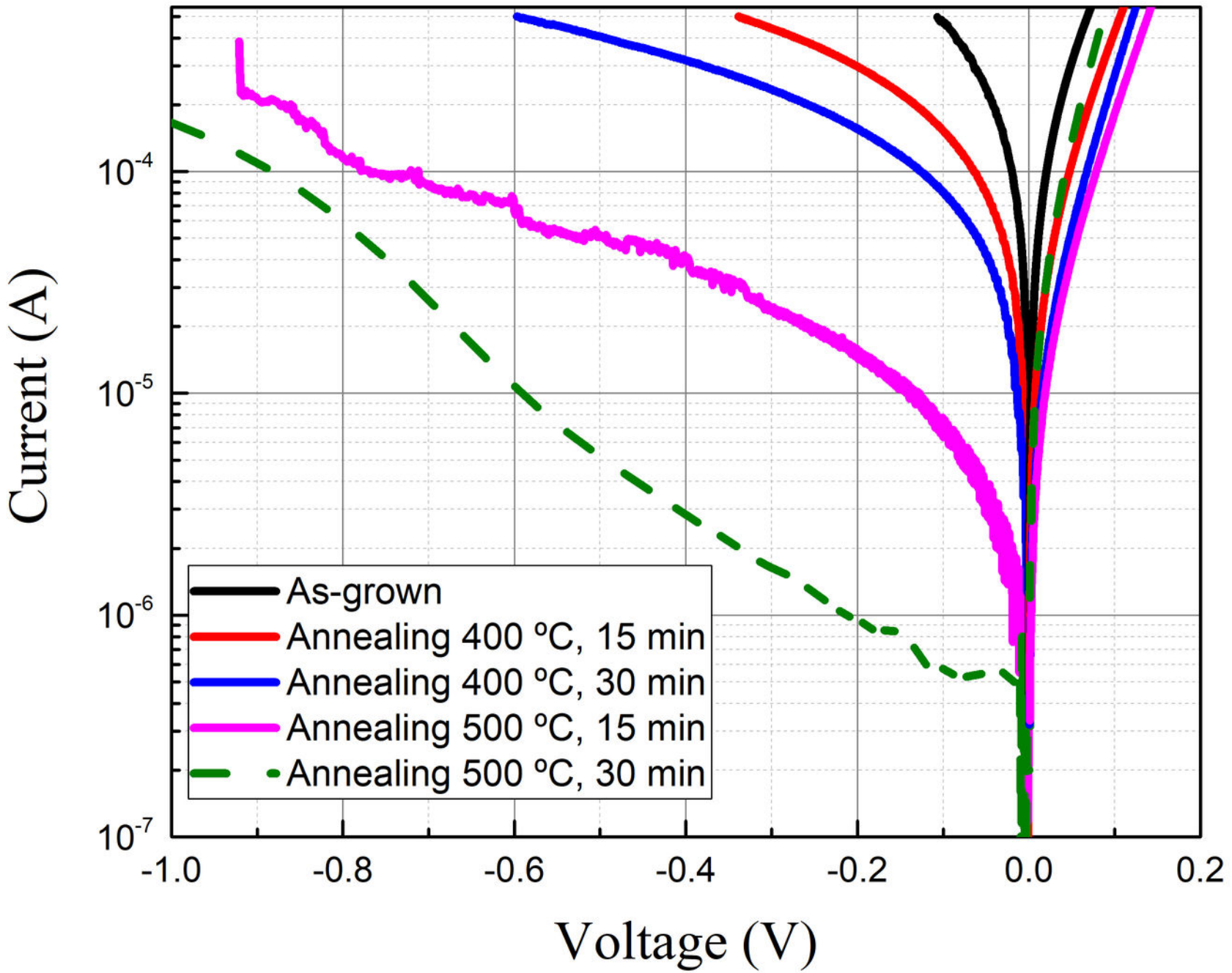
Current (A)
10-4
10-5
10-6
10-7
-1.0
-0.8
-0.6
-0.4
-0.2
0.0
0.2
Voltage (V)
As-grown
Annealing 400 ºC, 15 min
Annealing 400 ºC, 30 min
Annealing 500 ºC, 15 min
Annealing 500 ºC, 30 min

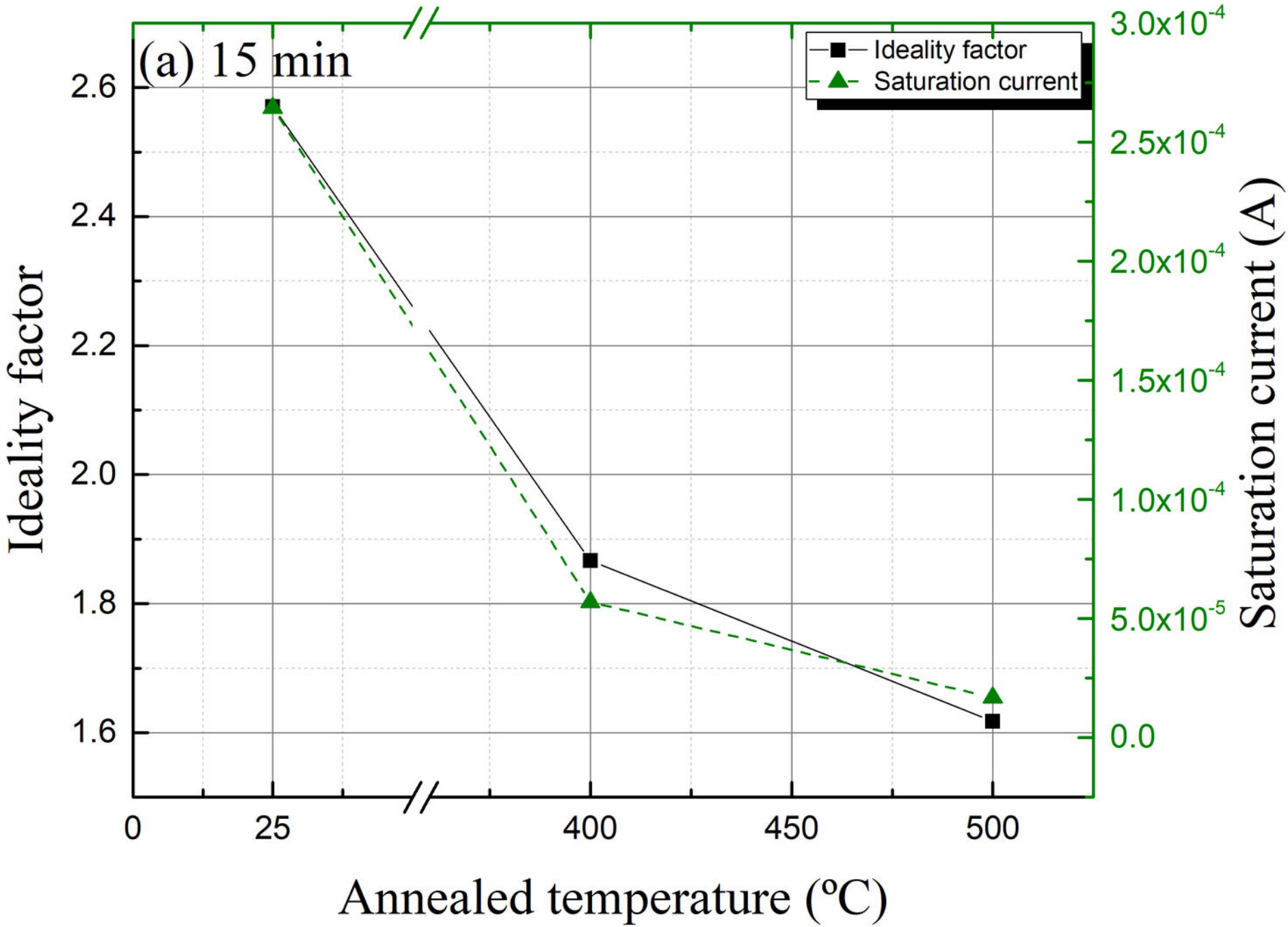
(a) 15 min
Ideality factor
Saturation current
Ideality factor
Saturation current (A)
Annealed temperature (ºC)
2.6
2.4
2.2
2.0
1.8
1.6
3.0x10-4
2.5x10-4
2.0x10-4
1.5x10-4
1.0x10-4
5.0x10-5
0.0
0
25
400
450
500

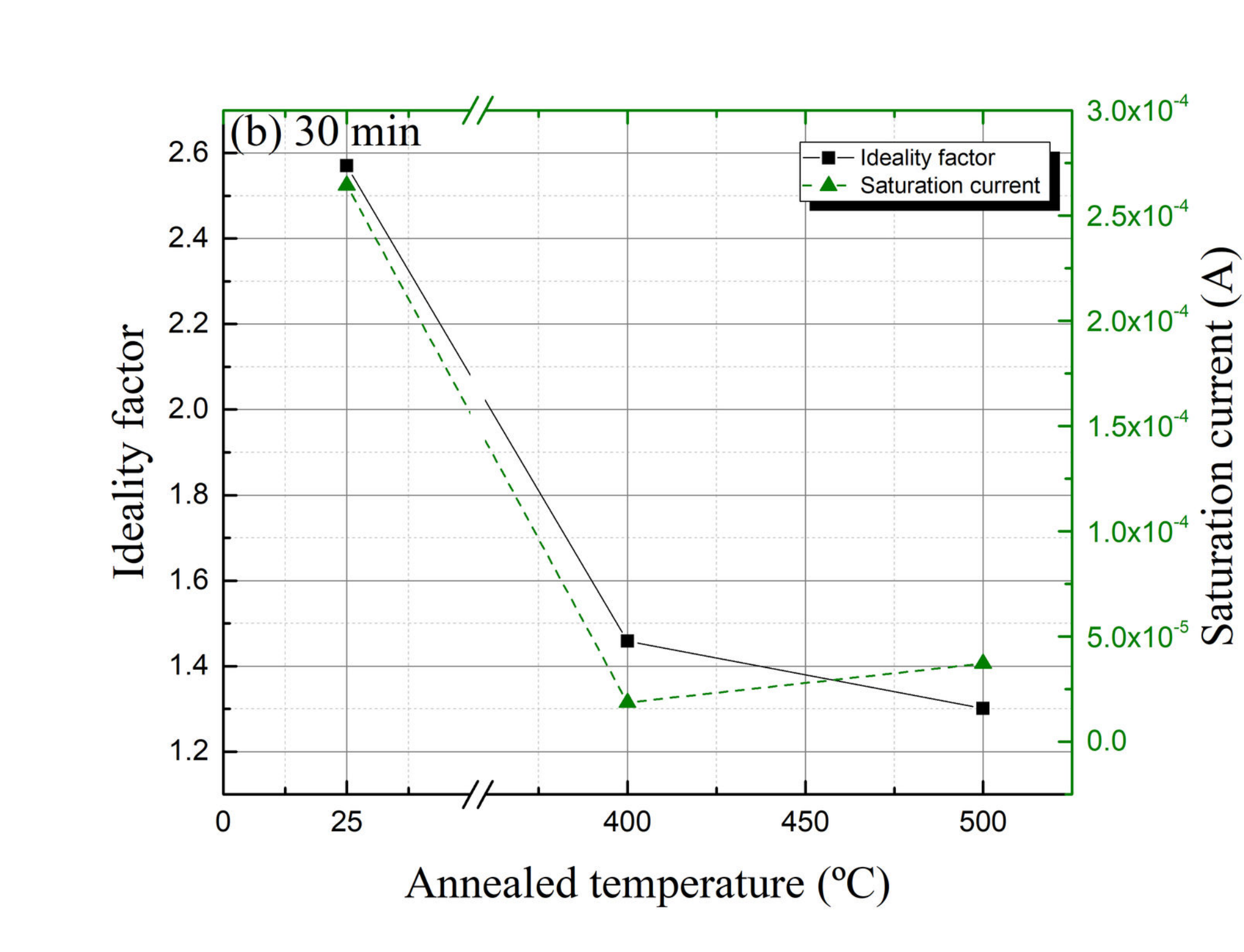
(b) 30 min
Ideality factor
Saturation current
Ideality factor
Saturation current (A)
Annealed temperature (ºC)
2.6
2.4
2.2
2.0
1.8
1.6
1.4
1.2
3.0x10-4
2.5x10-4
2.0x10-4
1.5x10-4
1.0x10-4
5.0x10-5
0.0
0
25
400
450
500

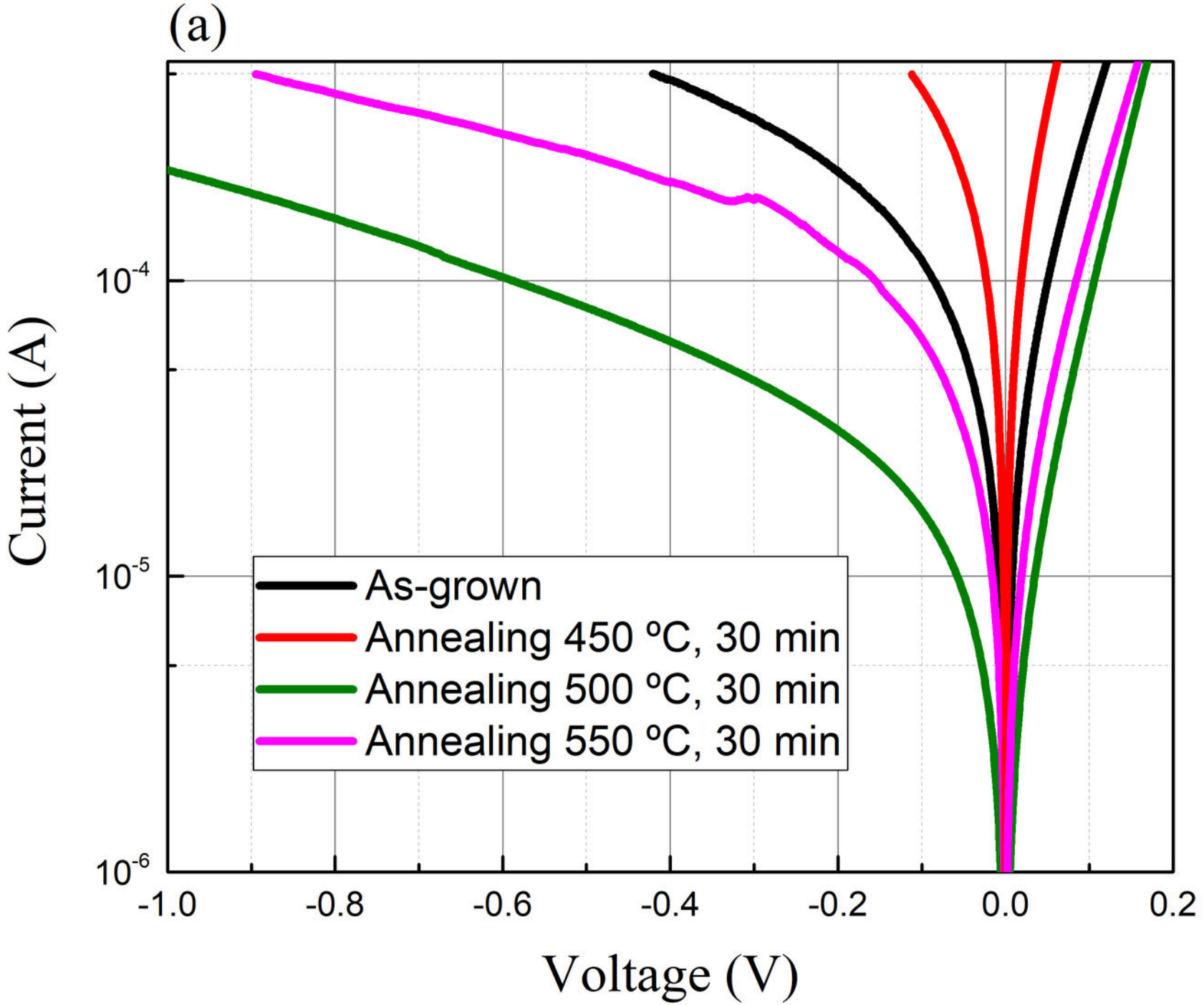
(a)
Current (A)
10-4
10-5
10-6
-1.0
-0.8
-0.6
-0.4
-0.2
0.0
0.2
Voltage (V)
As-grown
Annealing 450 ºC, 30 min
Annealing 500 ºC, 30 min
Annealing 550 ºC, 30 min

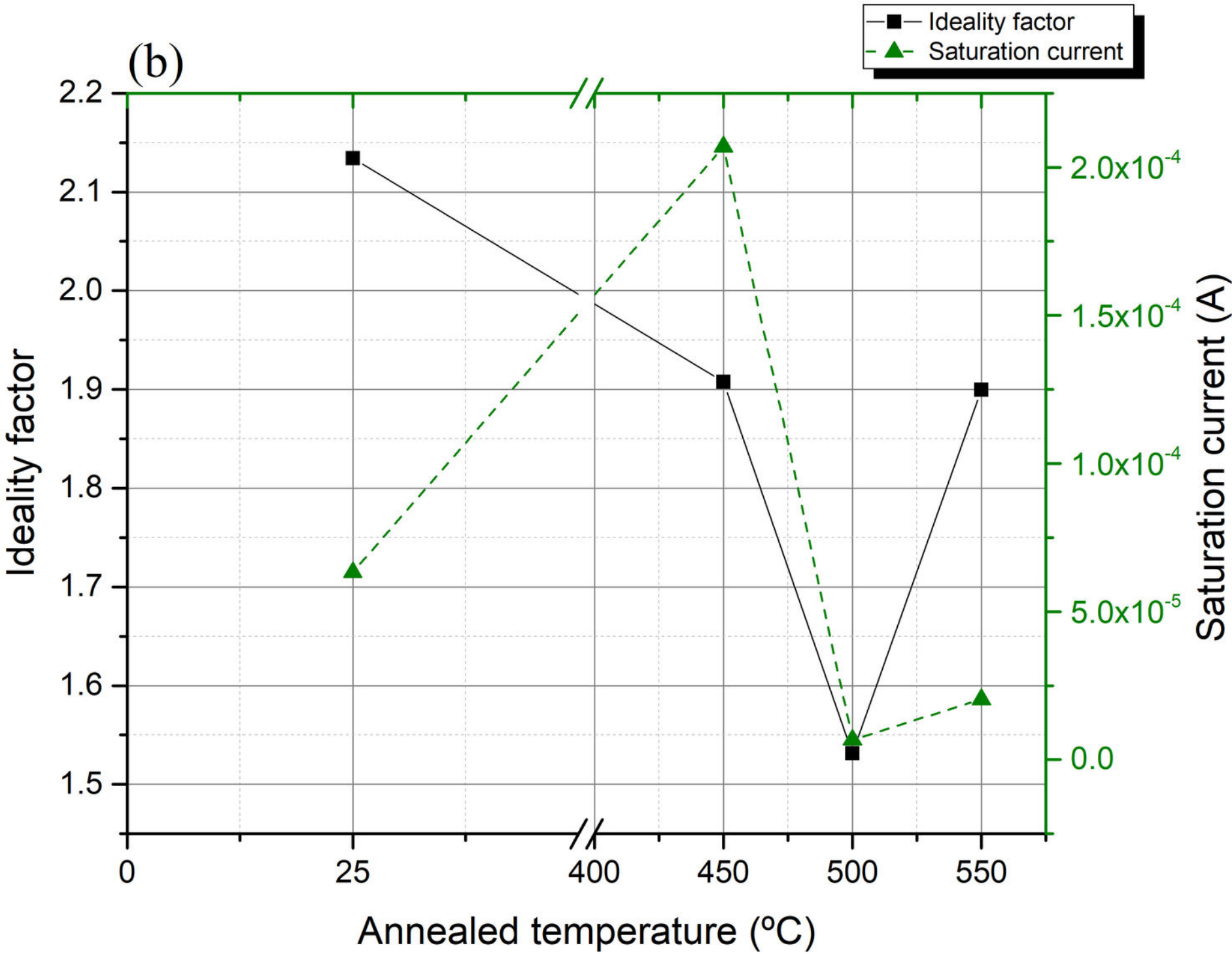
(b)
Ideality factor
Saturation current
2.2
2.1
2.0
1.9
1.8
1.7
1.6
1.5
Ideality factor
2.0x10-4
1.5x10-4
1.0x10-4
5.0x10-5
0.0
Saturation current (A)
0
25
400
450
500
550
Annealed temperature (ºC)

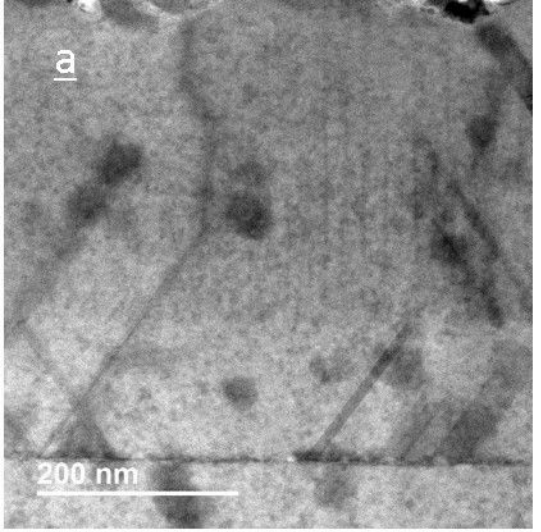
a
200 nm

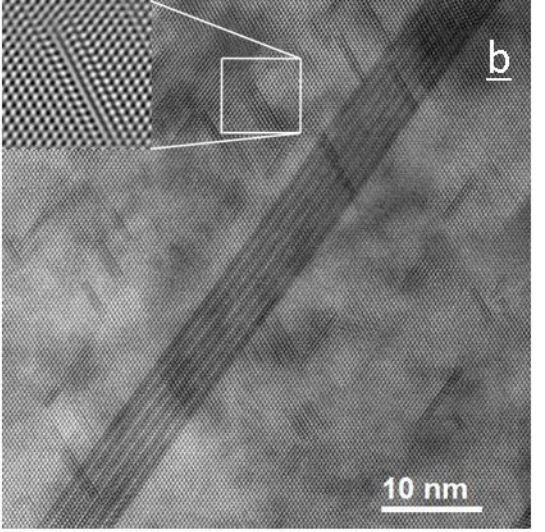
b
10 nm

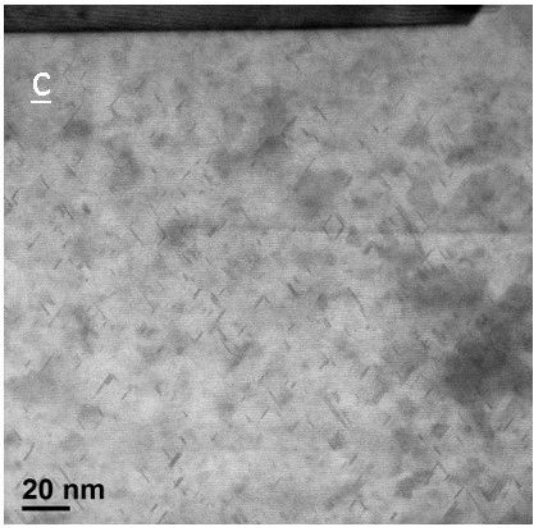
c
20 nm

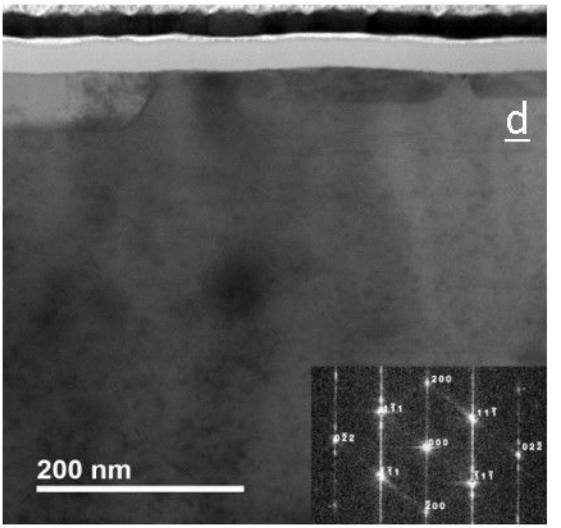
d
200 nm
200
022
000

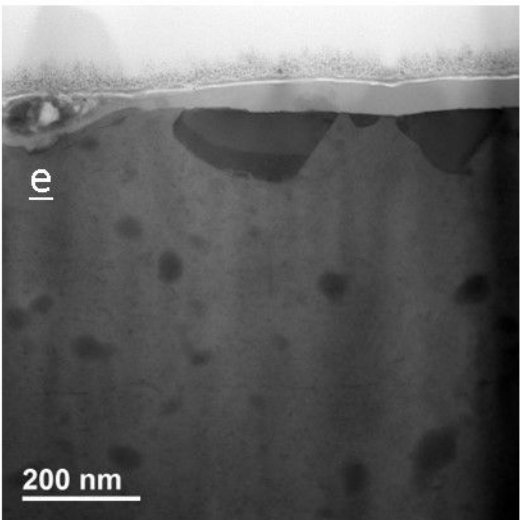
e
200 nm

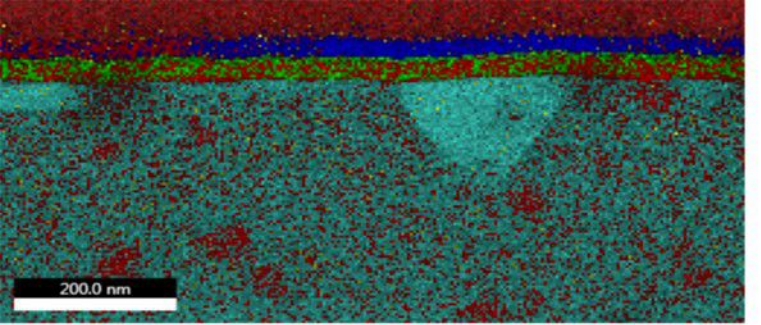

15% C K
8% O K
5% Bi M
33% Sb L
4% Cr K
24% Ga K
12% Au L